Merging toughness and oxidation resistance in a light ZrB2 composite

Silvestroni, Laura; Melandri, Cesare; Venkatachalam, Vinothini; Binner, Jon; Sciti, Diletta

DOI:
10.1016/j.matdes.2019.108078

Document Version
Publisher's PDF, also known as Version of record

Citation for published version (Harvard):
Silvestroni, L, Melandri, C, Venkatachalam, V, Binner, J & Sciti, D 2019, 'Merging toughness and oxidation resistance in a light ZrB_2 composite', *Materials and Design*, vol. 183, 108078, pp. 1-12. https://doi.org/10.1016/j.matdes.2019.108078

Materials and Design 183 (2019) 108078

Contents lists available at ScienceDirect

Materials and Design

journal homepage: www.elsevier.com/locate/matdes

Merging toughness and oxidation resistance in a light ZrB_2 composite

Laura Silvestroni [a,*], Cesare Melandri [a], Vinothini Venkatachalam [b], Jon Binner [b], Diletta Sciti [a]

[a] CNR-ISTEC, Institute of Science and Technology for Ceramics, Via Granarolo 64, I-48018 Faenza, Italy
[b] School of Metallurgy and Materials, University of Birmingham, B15 2TT Birmingham, UK

HIGHLIGHTS

- A functionally graded composite (FGC) based on ZrB_2 and 0 - 50 vol% short C fibres was obtained by hot pressing.
- The FGC overcome the trade-off between strength and toughness at high temperature achieving 10 MPa $m^{½}$ at 1500°C.
- The FGC withstood an oxyacetylene test at 2000-2500°C undergoing minimal recession.
- The FGC approach combines excellent failure tolerance and oxidation resistance in a lightweight material.
- The FGC hierarchical structure surpassed the resistance to damages and to extreme environments of traditional UHTCs.

GRAPHICAL ABSTRACT

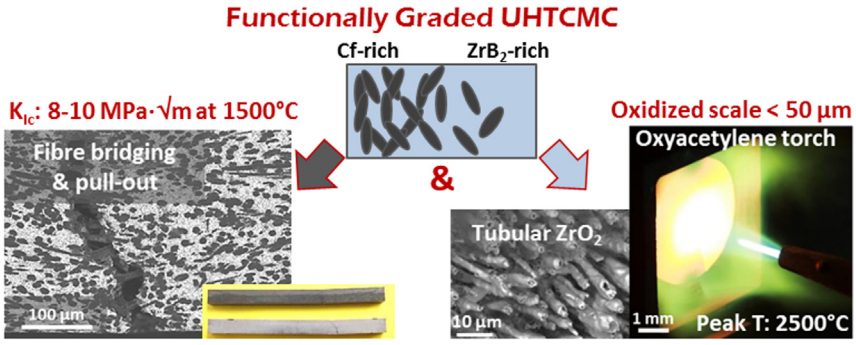

ARTICLE INFO

Article history:
Received 19 April 2019
Received in revised form 24 July 2019
Accepted 25 July 2019
Available online 26 July 2019

Keywords:
Functionally graded composite
ZrB_2
C fibre
Fracture toughness
Ablation resistance

ABSTRACT

A functionally graded composite based on ZrB_2 and 0–50 vol% of short carbon fibres was prepared via a deliberately simple approach that involved creating a suitable stacking sequence of layers with different sintering agents and fibre contents. This led to an excellent combination of failure tolerance and oxidation resistance in a light material with a density below that of alumina. The graded architecture outperformed other related composites when tested at 1500 °C and, separately, achieved a toughness of 10 MPa $m^{½}$. In addition, the composite withstood the ablation effect of an oxyacetylene torch at 2500 °C, undergoing minimal recession. Moreover, the true nature of the "tubular" zirconium oxide formed upon oxidation at extreme temperatures is reported for the first time. The functionally graded concept applied to a ultra-refractory matrix seems to be a promising route to obtain even complex shaped components with functional symmetry for use in severe environments.

1. Introduction

Zirconium diboride, ZrB_2, is considered to be one of the most promising materials in the field of aerospace hypersonic thanks to its combination of excellent refractoriness and ablation resistance [1–5], however, currently it has too many shortcomings related to its physical and structural properties and costly production to start actually being used. The main drawbacks of ZrB_2 and, in general, of all the transition metal borides, are their poor oxidation resistance, low fracture toughness and high density; the latter creating a significant weight penalty [1–5]. For the applications under consideration, the possibility of catastrophic failure and oxidation down to the material core are simply not options. The addition of functional phases, therefore, is considered to be one of the most favourable solutions to overcome these issues.

* Corresponding author.
E-mail address: laura.silvestroni@istec.cnr.it (L. Silvestroni).

https://doi.org/10.1016/j.matdes.2019.108078

As an example, it is known that the oxidation behaviour of ZrB_2 can be greatly enhanced with the addition of Si-containing phases, with silicon carbide, SiC, and transition metal silicides, $MeSi_2$, being the most commonly used additives [6–9]. The advantage of silicon-based phases occurs due to the formation of an outermost protective borosilicate glass that is more stable at high temperature than the boron oxide produced by bulk ZrB_2 upon oxidation. SiC is generally selected owing to its additional benefits on the mechanical properties [10–13], however it suffers from a transition from passive to active oxidation in the layer below the surface when the oxidation temperature exceeds ~1650 °C [14]. In contrast, appropriate $MeSi_2$ compounds can induce favourable changes in both the borosilicate glass formed, increasing its viscosity, and in the physical properties of the crystalline zirconium oxide also formed, in the latter case by the creation of eutectic melts. The result is the formation of oxygen diffusion barriers in the subsurface layers, protecting the ceramic core of the material [15–17]. Amongst the different $MeSi_2$ options, $MoSi_2$ has demonstrated that it is capable of improving the oxidation behaviour of diborides at temperatures up to 2000 °C [18,19].

In terms of the enhancement in toughness required to avoid catastrophic failure when the mechanical limit is exceeded, the introduction of fibres is the most common approach, although there are many parameters that must be considered including, amongst others, the chemical composition (SiC or C), degree of crystallinity (amorphous or crystalline), length (short or continuous) and architecture (random or uni- or multi-directional orientation) and the type of surface finish (as processed or coated with one or more of several different kinds of protective layers). Not all of these lists are suitable for increasing the fracture toughness and, in some cases, they can actually be detrimental. In general, significant fracture toughness increment can be achieved by introducing unidirectional carbon fabrics; values approaching 10 MPa $m^{½}$ have been attained [20,21], though the resulting anisotropic properties of the composite can become an issue. In this respect, the introduction of short random fibres, if distributed homogeneously, can yield consistent properties along the *xy* plane. The combination of UHTC matrices and SiC/C fibres has originated a new class of materials called ultra-high temperature ceramic matrix composites (UHTCMCs). It has been shown that short SiC fibres at the level of 10–20 vol% can double the fracture toughness of monolithic ZrB_2 [22], though at the expense of compromising the oxidation behaviour again due to the presence of the SiC, viz. the occurrence of active oxidation in the subsurface layers at temperatures >1650 °C. If this occurs, it is accompanied by the formation of large voids and hence the embrittlement of the overall structure architecture [23]. In contrast, the introduction of similar amounts of carbon fibre does not lead to a measurable increase in toughness for the composite compared to the monolithic ceramic, but just more controlled fracture has been observed [24–28]. In addition, the properties improve when the composite is tested at high temperatures, although, of course, the fibres must be protected in an oxidizing environment [29]. The possibility to add large amount of carbon fibres to a ZrB_2 matrix that lighten the composite and impart failure tolerance and at the same time preserving the ablation properties typical of UHTC would open a path to the development of innovative materials with unprecedented properties for use in extreme environments.

In light of all these considerations, it is clear that the introduction of a single phase cannot satisfy all of the structural and chemical requirements necessary to survive the extreme environment anticipated by the applications of these materials. Therefore, the addition of further, specific, functional second phases with a view to enhancing the mechanical or thermal aspects becomes desirable. In this context, the creation of a functionally graded composite, FGC, in which the composition changes gradually across the material has good potential for being a simple approach to maximizing the multi-phase benefits and minimizing their unfavourable side-effects [30–34]. For example, it has been shown that FGCs based on ZrB_2 containing up to 50 vol% of chopped SiC fibres have densities that are nearly half that of pure ZrB_2, display twice the fracture toughness compared to monolithic ZrB_2, whilst oxidation tests at 1650 °C did not harm the material thanks to tailored doping of the outermost protective layer [35]. Also an appropriate fibre/matrix interface was preserved during the various processing steps thanks to the graded introduction of different sintering agents. Considering the latter, sintering additives can on the one hand enhance matrix densification, whilst also potentially reacting with the fibres damaging their structure and hence their reinforcing effect [36]. This occurs, for example, in the case of $MoSi_2$, which strongly reacts with both SiC and C fibres during densification. Si_3N_4, in contrast, has a milder effect on fibre corrosion, but does not offer sufficient oxidation protection.

In this work, a simple method is proposed to fabricate functionally based composites with a ZrB_2 matrix containing short carbon fibres as both a reinforcing and mass-lightening phase. Based on the above arguments, use of the most appropriate sintering agent is critical throughout each area of the composite. Once made, the strength and toughness of the optimized composite were measured at up to 1500 °C in several directions in order to investigate the extent of any property variations. Then the FGC was exposed to an oxyacetylene torch to confirm its capability to withstand such an extreme environment. Compared to our previous study on ZrB_2 containing short silicon carbide fibres [35], here we use carbon fibres that enable to operate at much higher temperature without properties degradation. To prove the increased capabilities of this new FGC UHTC, we moved from oxidation in static furnace at 1650 °C [35], to an oxyacetylene torch that achieved the peak temperature of 2500 °C.

The hierarchical microstructure of the developed FGC surpassed the capabilities of traditional UHTCs in terms of resistance to damages, owing to the combined reinforcing action of the fibre and of suitable residual stresses between scales with different composition, and resistance to extreme environments, thanks to the tailored configuration of the outermost scale.

2. Experimental procedure

2.1. Materials preparation

The following commercial powders were used for the preparation of the mixtures for the FGC: ZrB_2 Grade B (H.C. Starck, Germany) with particle size range 0.6–4.7 μm, impurities (wt%) C: 0.2, O: 0.7, N: 0.10, Fe: 0.1, Hf: 1.7; $MoSi_2$ (Aldrich, Steinbeim, Germany) with particle size of <2 μm, purity99 + %, α-Si_3N_4 M11 (ABCR GmbH&CO, Karlsruhe, Germany) with mean particle size 0.15 μm, impurities (wt%) C: 0.2, O: 1.6, Al < 0.005, Co: 0.003, Ca: 0.001 and C chopped fibres (Granoc XN-80C-03S, Nippon Graphite Fibre, Japan) with 7–10 μm diameter and 200 μm length.

The ZrB_2 was doped with different agents depending on the specific function required of that part of the composite. The outermost layer, which was carbon fibre-free, contained 10 vol% $MoSi_2$ and was given the code ZB0-M. 8 vol% Si_3N_4 was added to the ZrB_2 as a buffer layer to hinder the diffusion of the $MoSi_2$ to the fibres located inside the composite where, as indicated previously, it can result in damaging attack; this composition was given the code ZB0-S. The same amount of additive was used to promote matrix densification in the material core where the fibres were located. The stepwise graded structure of the FGCs contained 0 to 50 vol% of C short fibres (code ZB20/30/50f) in a non-symmetric configuration, as sketched in Fig. 1.

Each ZrB_2/additive/fibre mixture was ball milled for 24 h in absolute ethanol using silicon carbide media. Subsequently, the slurries were dried in a rotary evaporator and the powders de-agglomerated. The mixtures were then weighed and poured into a 30 mm steel mould according to the stacking sequence displayed in Fig. 1 and uniaxially pressed at 25 MPa, perpendicular to the fibre length, in order to obtain sintered pellets of a suitable thickness for mechanical testing, e.g. around 3 mm. The 'green' FGC was hot pressed (Ing. Allaria, Turin, Italy) in low vacuum (~100 Pa) using an induction-heated graphite die

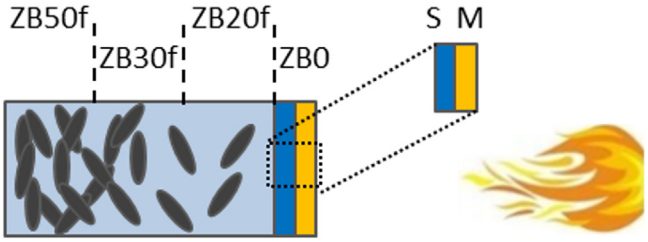

Fig. 1. Sketch of the FGC concept and stacking sequence.

with a uniaxial pressure of 30 MPa, which was increased to 40 MPa at 1900 °C. A holding time of 30 min was used. The furnace was slowly cooled down to 1000 °C to avoid cracking of the multi-layered structure, then the furnace power was turned off and the specimen was allowed to cool naturally.

2.2. Microstructure and mechanical characterization

The bulk density of the sintered pellet was measured by the Archimedes' method using deionised water as the liquid medium.

The microstructure was analysed on the surface and across the cross-section using field emission scanning electron microscopy (FE-SEM, Carl Zeiss Sigma NTS GmbH, Oberkochen, DE) and energy dispersive x-ray spectroscopy (EDS, INCA Energy 300, Oxford instruments, UK).

To account for the material anisotropy, one surface or the other of the FGC was machined off to an appropriate depth to reveal the layer to be characterized and allow the mechanical properties to be measured in different configurations, Fig. 2. The 4-pt flexure strength (σ) was measured at room temperature (RT) and 1500 °C in a partially protective argon atmosphere using the guidelines of the European standards for advanced ceramics, ENV843-1:2006 and EN820-1:2002. Chamfered bars with dimensions 25.0 × 2.5 × 2.0 mm^3 (length by width by thickness, respectively) were tested at RT using a 4-pt fixture (lower span 20 mm, upper span 10 mm) in a screw-driven load frame (Zwick-Roell mod. Z050, Germany) with a cross-head speed of 1 mm min^{-1}. The same machine was used, with an adapted furnace (mod. HTTF, Severn Furnaces Ltd., UK), to measure strength at high temperature in the partially protective Ar environment. Tests were carried out with both ZB50f and ZB0-M under tension (Fig. 2).

Fracture toughness (K_{Ic}) was evaluated using chevron notched beams (CNB). The test bars, measuring 25 × 2 × 2.5 mm^3 (length by width by thickness, respectively), were notched with a 0.1 mm-thick diamond saw; the chevron-notch tip depth and average side length were about 0.12 and 0.80 of the bar thickness, respectively. Toughness was evaluated considering 3 different configurations, e.g. with notch tip positioned in ZB50f layer, in ZB0-M layer and even in transversal mode with the notch falling in the central ZB30f layer, as represented in Fig. 2.

The specimens were fractured in the same facility used above at both room temperature and 1500 °C in partially protective Ar environment.

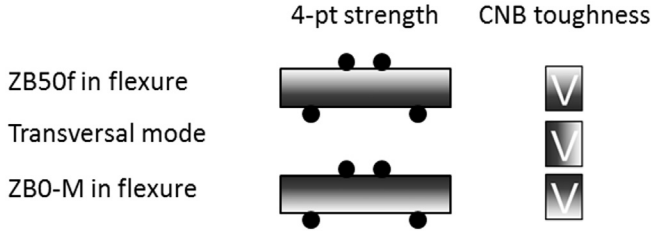

Fig. 2. Schematic illustrating the mechanical properties testing. The dark side represents layer with ZB50f composition, the white side represents the zero-fibre scale.

They were loaded with a crosshead speed of 0.02 mm min^{-1}. The "slice model" equation of Munz et al. [37] was used to calculate K_{Ic}. Note that before applying the load during both the strength and toughness testing at 1500 °C, a dwell of 18 min was used to ensure that thermal equilibrium was attained. For both temperatures, room temperature and 1500 °C, at least 3 bars were tested.

2.3. Oxyacetylene torch (OAT) tests

The resistance to oxidation at ultra-high temperature was studied using a custom built oxyacetylene torch facility at the University of Birmingham, UK, Fig. 3. The sample, one disc of 30 mm diameter and 4 mm thickness, was clamped during the test using screws and a holder made of G348 ultra-fine grain isostatic graphite (Tokai Carbon Europe, Warley, UK) and oriented at 90° to the torch flame direction at a distance of 30 mm to achieve a heat flux of 8.5 MW m^{-2}. The velocity of the flame has been measured by the Birmingham team as Mach 0.6 (~2060 ms^{-1}).

Sample mass and dimensions were measured before and after the sample was loaded into the graphite sample holder allowing the linear and mass ablation rates to be calculated. The fibre-free surface of the disc was exposed for 60 s to the oxidizing flame with an acetylene: oxygen nominal ratio of 1: 1.37. At the end of the testing period, the sample was gradually moved away from the flame to avoid cracking due to thermal shock. A thermal imaging camera (FLIR A655sc, SLIR systems AB, Sweden) and 2-color pyrometer (METIS M3, Sensortherm, Germany) logged the sample surface temperature as a function of time. The 2-color pyrometer (2-CP, Metis M3, Sensortherm) was capable of recording temperatures from 1000 to 3000 °C and the modified thermal imaging camera (TIC, FLIR A655sc) could record temperatures up to 2800 °C when combined with a neutral density filter. The back face temperature was recorded using a K-type thermocouple (Omega) attached to a data logger (YCT-747UD) and placed in contact with the sample through a hole drilled in the sample holder.

Microstructural changes were evaluated by SEM-EDS on both the surface and cross section whilst the thickness of the oxide layer formed was measured across the surface of the disc that was exposed to the torch, from side to side and passing through the centre, i.e. in the area most damaged by the flame. The topological characterization of the oxidized front and back surfaces was performed with a Contour GT-K 3D non-contact profilometer (Bruker, Germany) on areas measuring 10 × 25 mm^2 at the centre of each disc and the data was analysed using commercial software (Vision64 Map).

3. Results and discussion

3.1. Microstructure of the functionally graded composite, FGC

The structure of the FGC, consisting of a UHTC matrix containing short carbon fibre as reinforcement, is demonstrated in Fig. 4a, where the cross section displays a dense microstructure with regular fibre distribution across the sample depth and no cracks at the interfaces due to coefficient of thermal expansion mismatch. The thickness of the various layers was homogeneous and compatible with the specimens required for mechanical tests (e.g. 2.5 mm), specifically ZB0-M: 150 μm, ZB0-S: 150 μm, ZB20f: 600 μm, ZB30f: 600 μm and ZB50f: 1000 μm. The final density was 3.87 g/cm^3, with an overall fibre content around 33 vol%.

Details of the microstructural features of each layer after sintering are shown in Fig. 4b–f. The outermost layer resulted in a multi-layered structure, with a gradual impoverishment of $MoSi_2$ going towards the ceramic surface and core, as confirmed by EDS elemental mapping, Fig. 5. The outermost 100 μm was composed of a fully dense microstructure containing mostly MoB, with bright contrast, and darker SiC particles, Fig. 4b. These are common products deriving from the reaction of the $MoSi_2$ with the oxides on the surfaces of the precursor powders followed by reduction at high temperature in the carbon-rich sintering

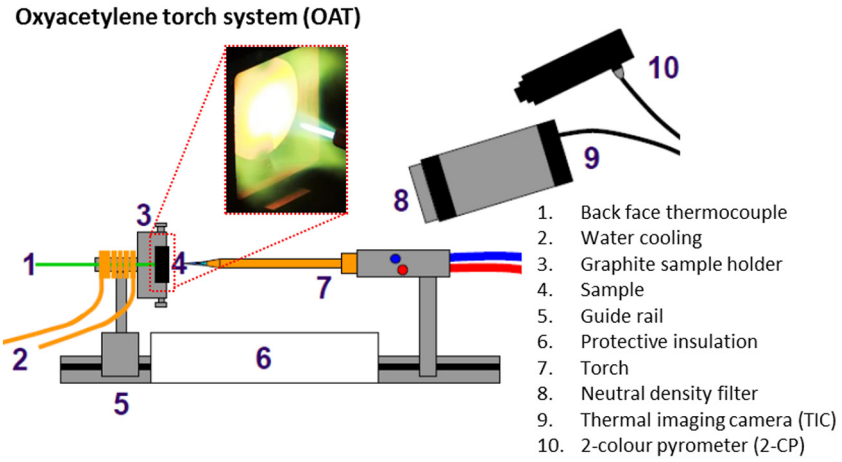

Fig. 3. Schematic of the oxyacetylene torch experimental set-up.

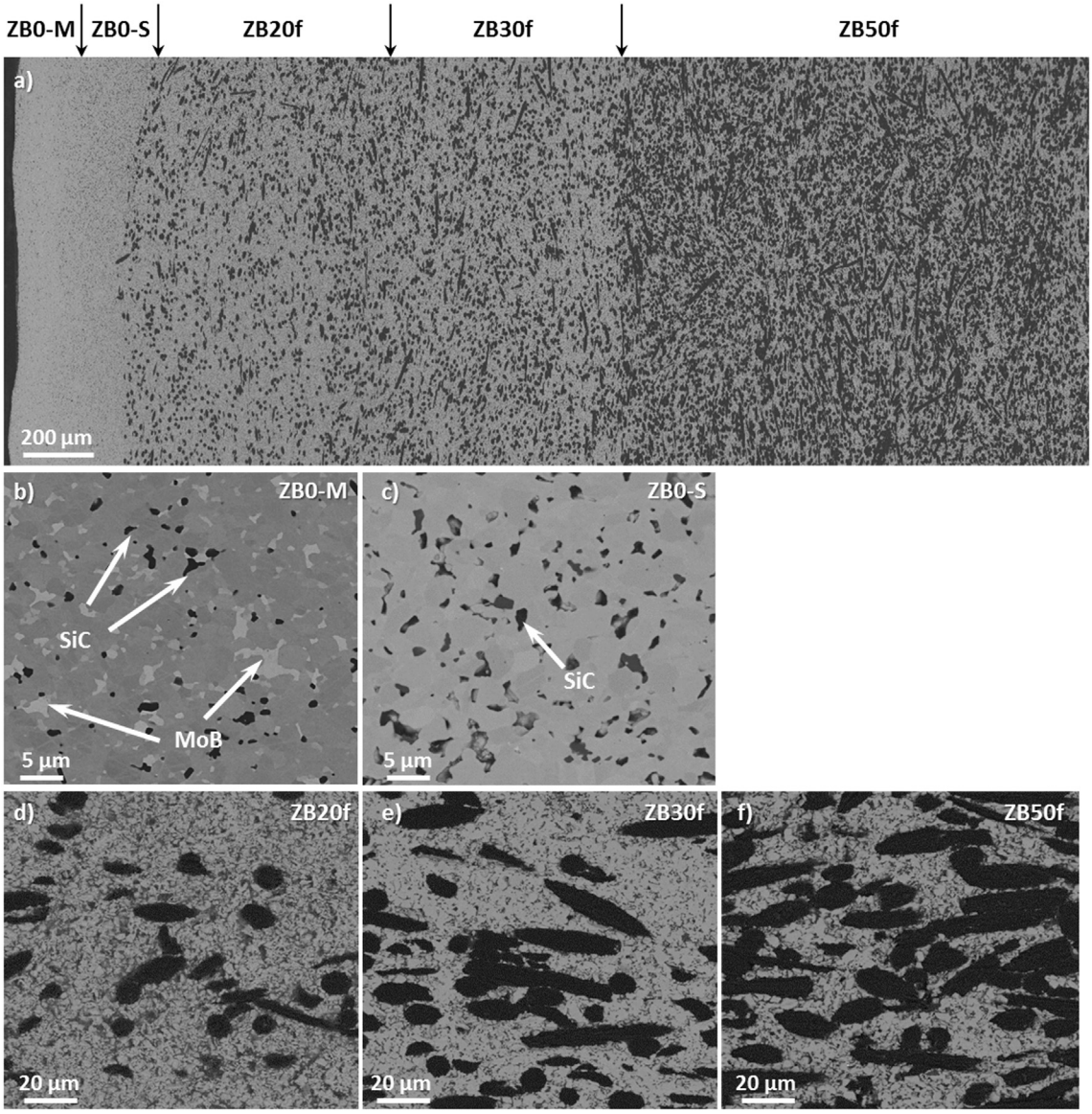

Fig. 4. SEM images of the functionally graded ceramic, FGC, showing a) the overall cross section and b)–f) magnified views of each layer.

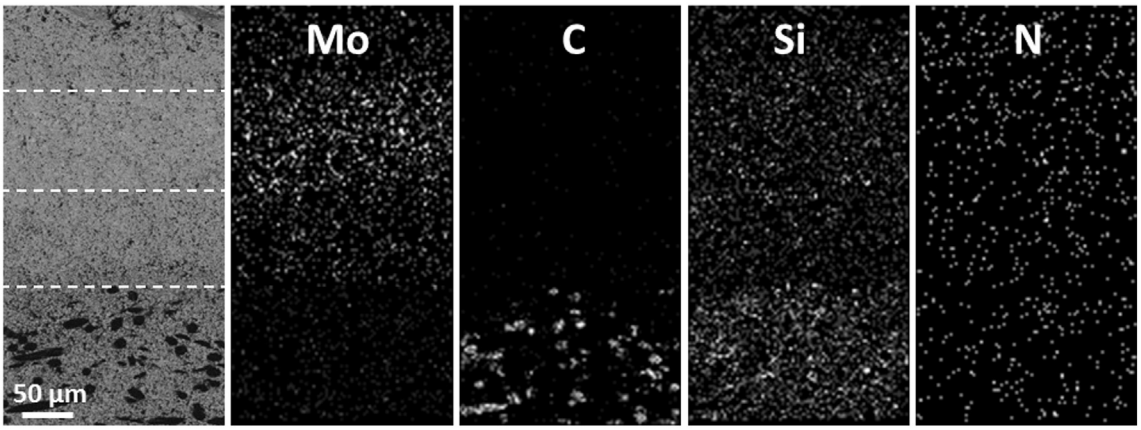

Fig. 5. SEM image of the cross section of the FGC in the UHTC-rich region and elemental distribution in the corresponding EDS maps.

environment that existed close to the graphite piston, [4,5,18] according to reactions (1) & (2):

$$2MoSi_2 + B_2O_{3(g)} + 2.5O_{2(g)} \rightarrow 2MoB + 4SiO_2 \quad (1)$$

$$SiO_2 + 4CO_{(g)} \rightarrow SiC + 3CO_{2(g)} \quad (2)$$

Inside the ZB0-M layer, the presence of unreacted $MoSi_2$ was observed, as revealed by the elemental mapping shown in Fig. 5; this was followed by the ZrB_2 layer containing Si_3N_4, ZB0-S. Within this layer, mainly SiC and low density Si-O-B-N phases were found in the final microstructure, Fig. 4c, owing to densification reactions extensively described in previous work [38]. Nitrogen-based phases were homogeneously diffused through the first 400 μm owing to their high diffusivity as melt phases at such high sintering temperatures. What is important to note is that effective blockage of the Mo-based compounds was successfully achieved by the introduction of the intermediate ZB0-S buffer layer and, accordingly, no Mo-compounds were detected within the fibre-based layers at any depth level.

However, in the first tens of micrometre thickness of the ZB20f layer, a slight modification to the fibres occurred, as revealed in Fig. 6a. The relatively high abundance of Si-based melt running across the particles and fibres during the densification stage filled the voids in the most porous zone by capillary forces and hence surrounded the fibres. As a result, the final fibres displayed a multi-layered morphology with a carbon core surrounded by a reaction layer composed of SiC, resulting in the fibres having an overall irregular and jagged cross-section. Further in to the centre of the FGC, however, the fibres continued to exhibit their normal round shape and the typical multi-sheet morphology peculiar to pitch-derived fibres, Fig. 6b.

The matrix of composite, composed of layers of ZrB_2 containing different amounts of chopped fibres, the ZBxf layers, had residual porosity that increased with increasing fibre content, i.e. negligible up to 30 vol% fibre, around 10 vol% in ZB50f layer. In addition, the matrix was progressively depleted in SiC; see Fig. 4d–e. It is plausible that the liquid Si-based phase in the fibre-rich layers was progressively consumed by carbo-reduction through reaction with the carbon fibres during sintering, so that increasingly lower amounts of liquid phase, and with increased viscosity, was available for the precipitation of SiC particles in the matrix and around the fibres. Accordingly, the SiC domains around the fibres in ZB50f were much thinner than those in the ZB20f layer. However, the fibre/matrix interface was generally weak throughout, as commonly observed for such composites containing this type of fibres [24].

3.2. Mechanical properties

As mentioned previously, the mechanical properties were determined in several directions to account for the expected composite anisotropy, Fig. 2, and then compared with data obtained using the same conditions and facility from other mono-reinforced ZrB_2 composites containing short C fibres in amounts ranging from 5 to 50 vol% [24,39].

The room temperature four-point bending strength was measured, separately, with the ZB0-M layer in both tension and compression yielding values of 82 ± 2 and 130 ± 3 MPa, respectively. Both are in line with the trend expected values for materials containing a global level of about 33 vol% fibre, Fig. 7a, and are of the same order as for ZrB_2-composites reinforced with a high volume fraction of short or continuous fibres [24,39]. Indeed, the introduction of a high volume fraction of fibre changes the defect population and notably decreases the

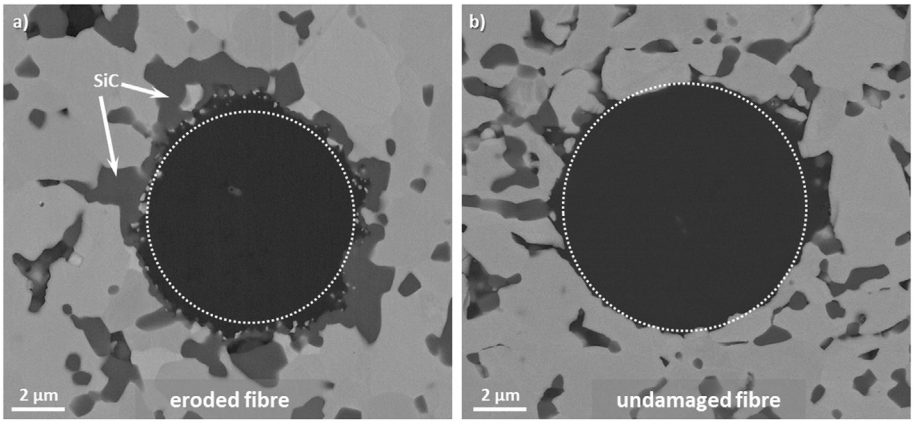

Fig. 6. SEM images of the fibres in the reinforced area of the FGC and showing a) significant and b) negligible edge corrosion after sintering in Z20f and ZB30f, respectively.

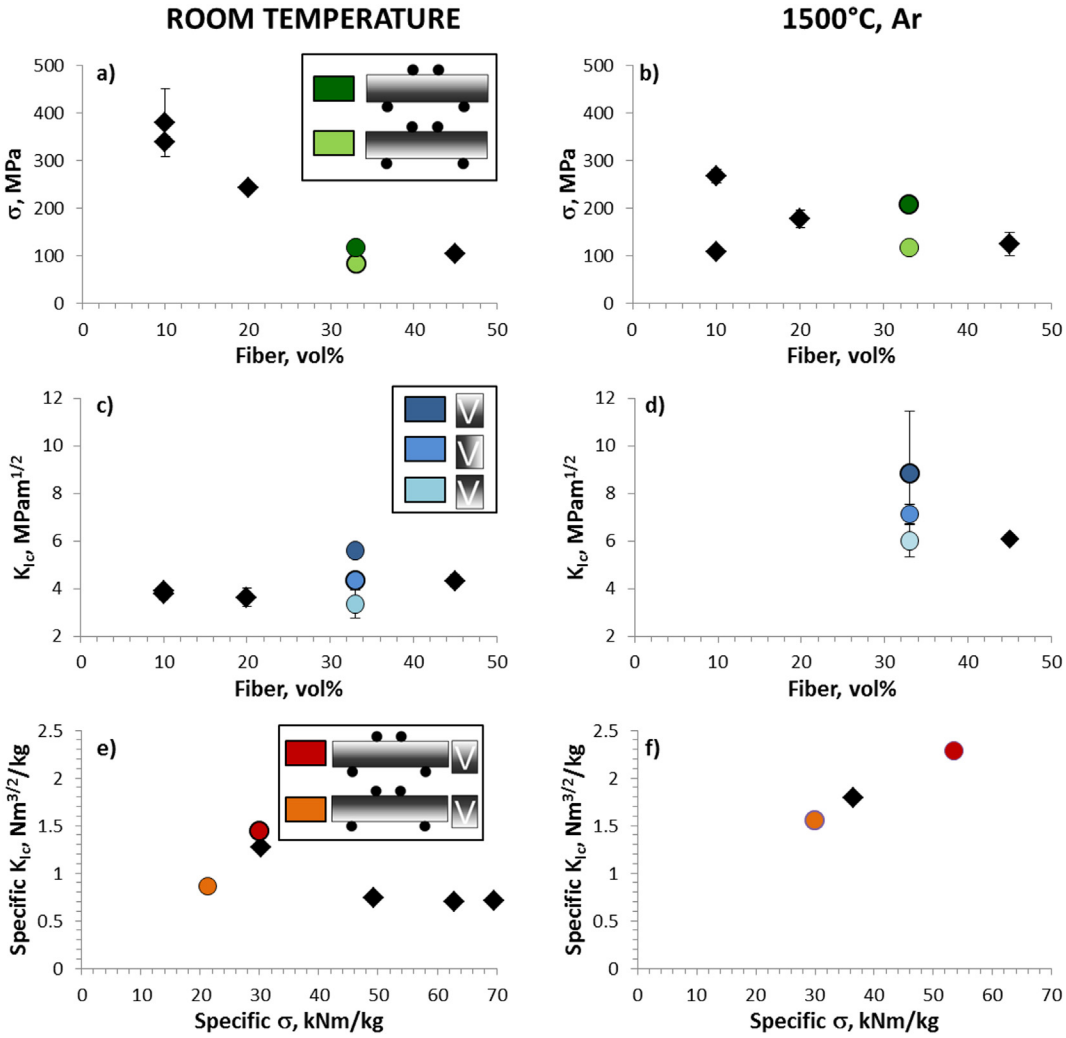

Fig. 7. Plots of the mechanical properties of the FGC measured at room temperature (left) and 1500 °C in Ar (right) in different configurations and compared to mono-reinforced composites (black symbols) [24,39]. The legend inset in (a, c, e) sketches the bending direction for both mechanical properties. Dark side identifies the ZB50f layer, the white side identifies the ZB0-M layer. Error bars are in some cases hidden by the corresponding marker. (For interpretation of the references to color in this figure legend, the reader is referred to the web version of this article.)

strength due to the higher fraction of fibre ends and the interactions between them. This can cause stress accumulation and micro-cracks to develop at the interfaces, which can merge together into larger cracks. It should also be mentioned that the composites surfaces, which did not contain any fibres, contained shallow machining flaws, which will have also contributed to the relatively low strength values measured. Another source of weakness for the unreinforced external ZB0-M layer comes from the inevitable development of residual stresses upon sintering. Layers containing fibres have a lower CTE compared to the fibre-free ZrB_2-$MoSi_2$ layer. Therefore, the external ZB0-M layer will

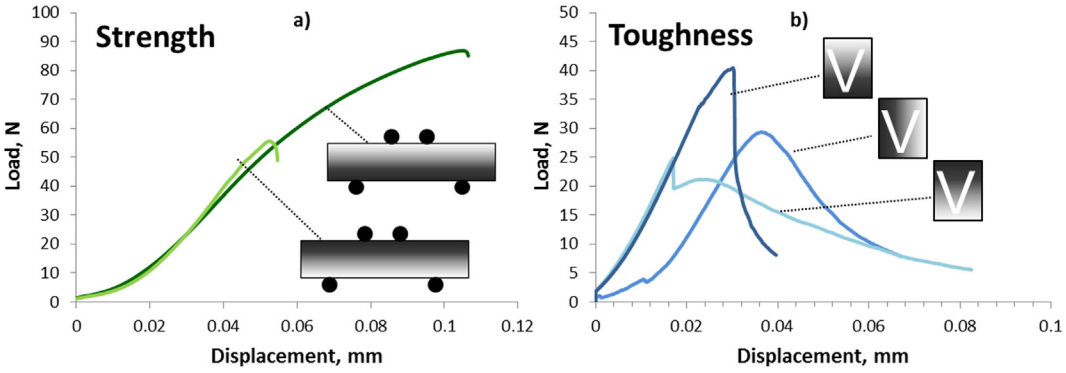

Fig. 8. Load displacement curves for a) strength and b) toughness of the FGC tested at room temperature in different configurations as sketched. Dark side identifies the ZB50f layer, the white side identifies the ZB0-M layer.

be under tensile stress after sintering, whilst on the opposite side, ZB50f will be in a state of compression. For this reason, the configuration in which ZB50f is under tension in the strength test is likely to give higher values of the ultimate stress (dark green), compared to the opposite configuration (light green), see Fig. 7a.

The load-displacement curves shown in Fig. 8a show a small controlled drop before failure, suggesting a slight degree of fibre pull-out immediately prior to fracture. It is also noteworthy that, in any configuration and at any temperature, the strength bars did not break into separate pieces, as shown in Fig. 9a. Indeed, SEM observations along the crack confirmed extensive fibre bridging and pull-out, Fig. 9b,c.

The fracture toughness measurements yielded quite a broad range of values; higher when the notch fell in the fibre-rich region and lowest when it fell close to the zero-fibre region, Figs. 7c and 8b, as expected. It is worth noting that, when tested in the most favourable configuration, the FGC was notably tougher than a mono-reinforced composite containing 45 vol% of fibre, Fig. 7c, and more than one and a half times tougher than un-reinforced ZrB_2 monolithics. Another interesting feature was the failure mode observed during the chevron-notch tests, in any configuration. For the mono-reinforced ceramics containing a fibre volume amount of 10–20%, no increase of toughness was measured although the load-displacement curves revealed controlled failure [24,39]. In the present work, the FGC simultaneously achieved a higher load before rupture and a more tolerant failure profile, i.e. after the first crack formed, a small drop in load followed and the curve assumed a tail shape typical of stable crack propagation, Fig. 8b.

However, the most appreciable structural improvement of the FGC architecture was revealed during testing at 1500 °C, both in terms of strength and toughness, Fig. 7b,d. In the most favourable configuration, the strength was almost double that commonly observed for analogous composites [24] and is attributed to the partial oxidation of the SiC particles, leading to healing of the surface flaws and to the release of the stress accumulated during processing. In particular, the toughness measurements made in the configuration with a high fibre concentration gave an average value of around 8.8 MPa $m^{½}$, with single values exceeding 10 MPa $m^{½}$. Such high fracture toughness values have previously been achieved only in composites based on unidirectional continuous fibre layup [21] or with a coating applied on the fibres [20]. Although comparative data for fracture toughness measured at high temperature are still very scanty, this architecture seems to be a viable, cheap and effective solution to the challenge of creating damage tolerant materials based on brittle UHTC matrices. Plots of the specific toughness and strength, Fig. 7e & f, further underline that, especially at high temperature, the apparently unavoidable trade-off between strength and toughness can actually be achieved with such an architecture. This is possibly due to the exploitation of the favourable residual stresses arising between layers of different composition.

Future activity will focus on the optimization of the composite properties, in terms of both thickness and composition of each layer within the FGC architecture, through a-priori simulation. For example, finite element modelling or weight function analysis could help to predict the toughness of the FGC as a function of the crack tip location and to the design of different stacking sequences [40,41] with the aim of designing such easy to fabricate, layered composites with enhanced failure tolerance.

3.3. Oxidation behaviour

Pictures of the FGC disc before, during and after the oxyacetylene torch (OAT) testing are shown in Fig. 10a. The dark features on the front face of the disc prior to testing are due to small residual amounts of the carbon foil used during hot pressing. A picture taken during the test shows a yellowish halo outgassing from the disc, which could be due to MoO_3 vaporization. After the test, the front face shows a damaged, central, white-yellowish region and a dark periphery. Whitening of borides is related to their transformation into crystalline oxides, whilst a darkening is associated with the development of an outer layer of silica-based glass. The back-face also developed a whitened central spot where the temperature had been high enough to cause oxidation to occur.

The temperature of the front surface of the composite (ZB0-M) was monitored by both TIC and 2-CP and, generally, the 2-color pyrometer gave values that were slightly higher than the infra-red camera. The temperature achieved in the centre of the disc was 2190 °C and was held for 60 s, however, in the last 10 s a temperature jump occurred resulting in a brief peak temperature of ~2500 °C in the very central area, as shown in the thermo-camera profile temperature and screenshot in Fig. 10b & c. Temperature jumps are often measured upon testing of related materials under extreme conditions and have been generally associated with a transition in surface chemistry,

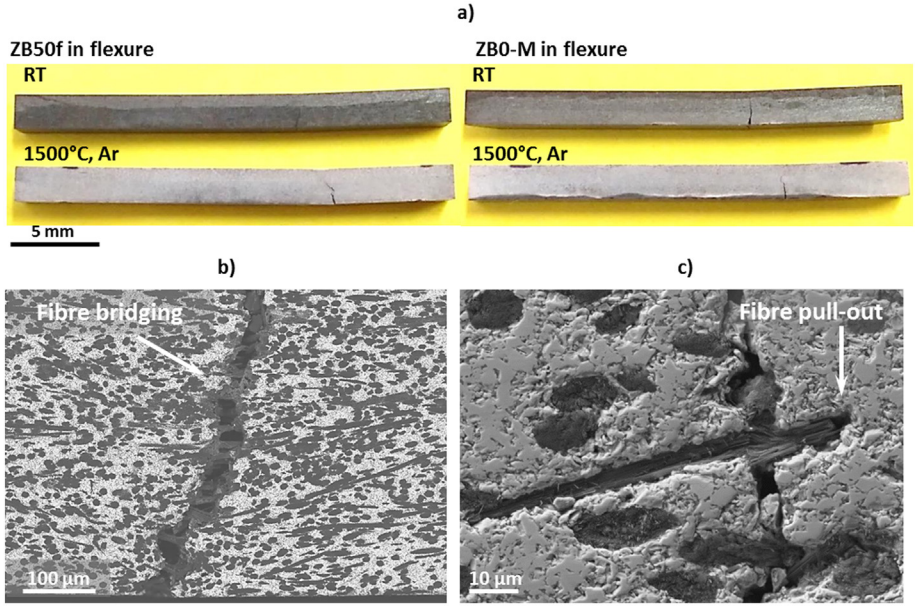

Fig. 9. a) Images of the strength specimens after testing at room temperature and at 1500 °C. b) and c) SEM images of fractured samples at room temperature with ZB50f in flexure showing extensive fibre pull-out.

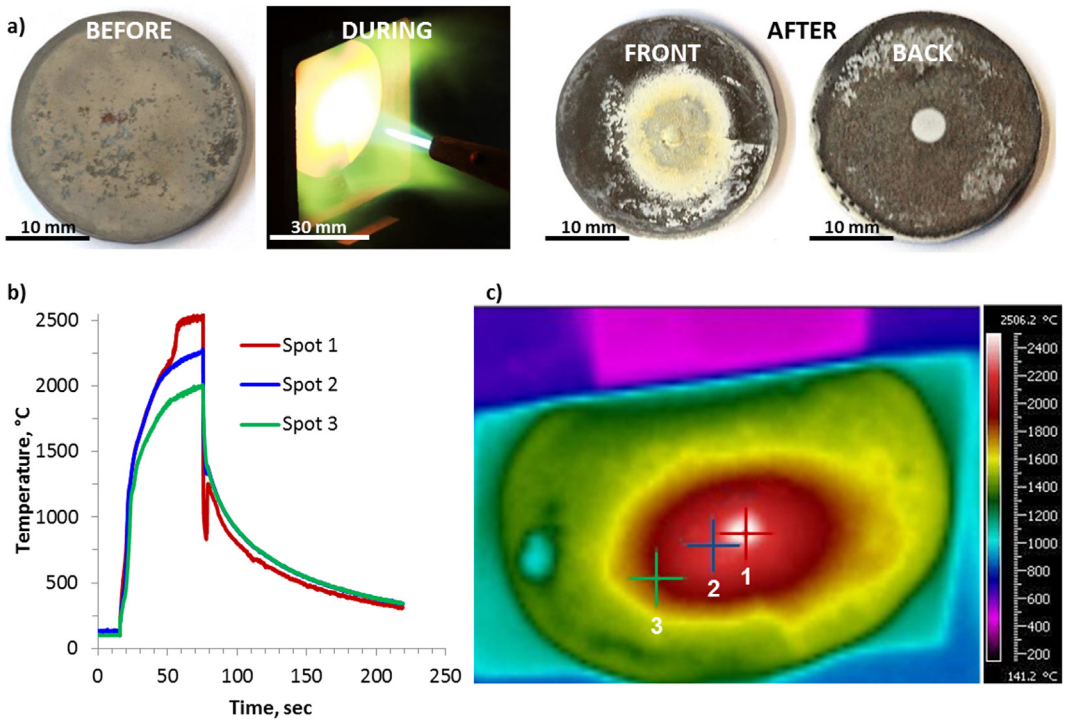

Fig. 10. a) Pictures of the FGC disc before, during and after the torch test on the front and back faces. b) Temperature profiles measured on the front surface by thermal imaging camera (TIC) in the three locations indicated in c).

[42,43] e.g. a loss of a protective silica glass and a resulting dramatic reduction of the thermal conductivity in the oxide scale. The back face temperature measured on ZB50f by a K-type thermocouple was 584 °C, which is a relatively high temperature probably related to the high conductivity of the unoxidized composite.

The mass and thickness change were measured, with corresponding rates of −0.0003 g s^{-1} and 0.004 mm s^{-1}. The thickening of the sample will have been due to oxide formation, whilst the small mass loss will have been because the escape of volatile species, such as SiO, MoO_x, B_xO_y, exceeded (slightly) the gain in mass arising from oxidation.

Fig. 11 shows the topography maps of the front and back faces to appreciate the new asperities formed on the disc by the highly thermoablative test. The topographic map of the front face reflects the degree of damage that the disc underwent, with features such as craters, bubbles and spikes being formed, whilst a more homogeneous surface was naturally observed for the back face, where the green circumference identifies the edges of the region that experienced almost 600 °C.

An X-ray diffraction pattern of the front surface after testing, Fig. 12, showed monoclinic zirconia to be the main phase as expected. Some peaks of borides including ZrB_2 and MoB were also clearly identified, suggesting the level of oxidation was just a thin scale that did not block the boride signal from beneath.

The front surface was also analysed by SEM-EDS and Fig. 13a shows an overview of the microstructure. Each of the areas highlighted, (b) to (h), are shown in greater detail below. Moving in from the edge, Fig. 13b, B_2O_3 thin crystals cover a partially porous ZrO_2 distinguished by a fine grain size and discontinuous pools of silica. Then there is a rough continuous glassy phase, Fig. 13c, which also incorporates ZrO_2 crystals. The next region is a smooth and homogeneous SiO_2 glass with ZrO_2 precipitates, Fig. 13d, which precedes another zirconia-rich region that evidently underwent densification, Fig. 13e and which is interrupted by a glassy phase that shows evidence of turbulence, segregation and the precipitation of ZrO_2 and other impurities, Fig. 13f. This latter region marks the edges of the extremely hot zone where the flame made direct contact with the sample. In this central area, globular zirconia spheres, as large as 40–100 μm, are scattered throughout a continuous glassy phase, Fig. 13g, whilst a higher magnification view reveals micro hollow tubes covering the entire region. This is presumed to be the well-known "columnar zirconia", often observed by the UHTC community on the surface of samples oxidized at very high

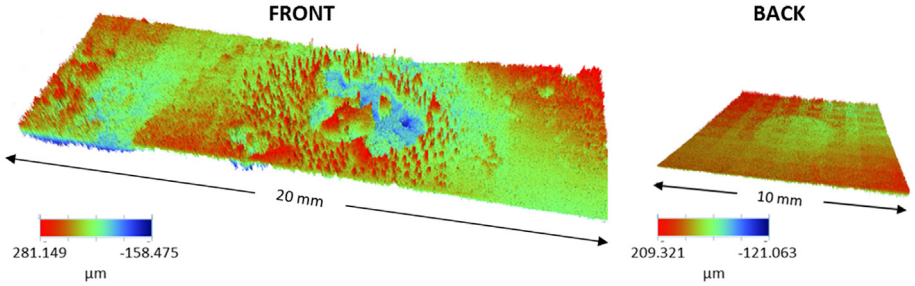

Fig. 11. Topographic maps of the front and back face of the disc after OAT testing. The grid visible in the back face is a software artefact.

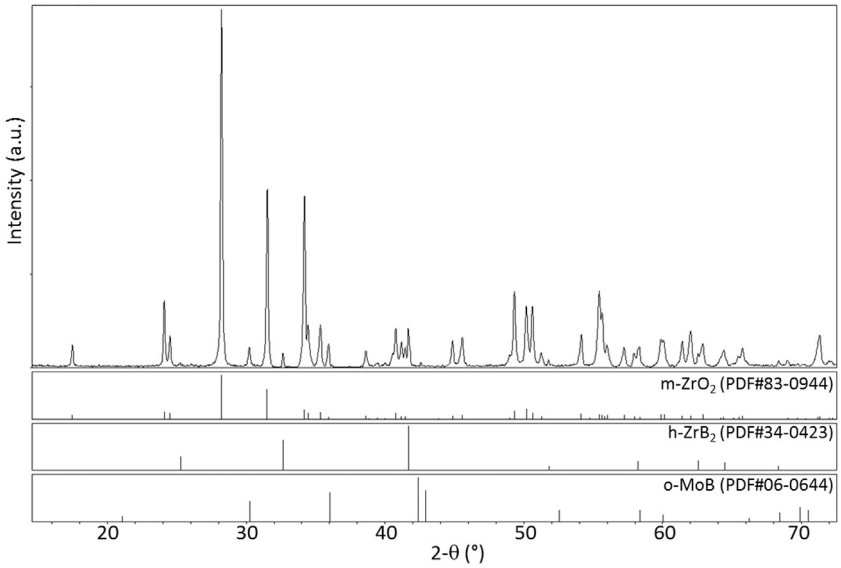

Fig. 12. X-ray diffraction pattern of the front-face of the disc after OAT testing at ~2190 °C for 60 s.

temperatures [8,44–47]. Here, for the first time, we demonstrate it to be actually a tubular form of zirconia. In the very centre of the disc, an area of ~2.2 mm in diameter, melted zirconia grains and silica are found, Fig. 13h. The zirconia shows irregular jagged edges, both in contact with the glass and where grains are adjacent to each other, suggesting rapid solidification from a liquid phase. Indeed, the presence of melted zirconia grains would suggest the formation of an eutectic phase, which cannot to be excluded given the sudden increase in temperature, to ~2500 °C, achieved in the centre of the disc in the final few seconds of testing.

Cross sectional analysis revealed that, as expected, the oxidized layer was limited to a thin layer of the fibre-free UHTC and the oxide profile was inhomogeneous, being thicker in the centre, about 45 μm, and thinner at the edges, about 10 μm, Fig. 14a. In the region of the central crater shown in Fig. 13a, the cross sectional analysis showed that the coarser oxide layer detached leaving a thin, adherent oxide coating. The composition of the modified scale was in agreement with previous studies [18]; above the unreacted bulk, a ZrB_2-MoB-SiO_2 scale was found, with MoB and SiO_2 following the shape of the original $MoSi_2$ aggregates according to reaction (1). Moving further towards the surface in the central zone, the SiO_2 disappeared leaving region of partially porous, equiaxed ZrO_2 grains decorated with tiny MoB aggregates, Fig. 14b (bottom). The oxide/boride interface in this very damaged region was very sharp and not well adherent, probably owing to the martensitic transformation of the ZrO_2 that will have occurred on cooling from the testing temperature and the volume variation associated with it. Above it, the dense scale of ZrO_2 contained grains of entrapped MoB, Fig. 14b (top), presumably as a result of the vigorous action of the very high velocity of the gases making up the flame. The morphology of the MoB phase in these porous and dense regions varied, as appreciated from the insets in Fig. 14b; first it is in the form of isolated aggregated particles and then it assumes a more continuous 'lace-like' structure. Unfortunately, the level of oxygen contamination is hard to define owing to the limited spatial resolution, however, it is plausible to attribute such morphology change to a partial oxidation. As the oxygen partial pressure increases nearer to the surface, the MoB becomes richer in oxygen and progressively melts [48]. Right at the top, only ZrO_2 was present, first in form of hollow tubes, then as large lumps that were filled with fine grained ZrO_2 and silica-based glass, Figs. 14c and 13g. Such well-defined tubes were never reported before and testify to the great amount of vapours and volatile fluxes, mostly boron oxide, generated upon oxidation of the boride at such hot temperatures. The large ZrO_2 bulges spread out in the "g" zone in Fig. 13 are possibly a result, again, of the turbulent effect of the very high gas velocities resulting in explosive forces and oxide fragmentation in the central region.

Investigations on the back surface revealed that a 2 mm diameter dimple was formed matching the region where the region of highest flux was observed on the front surface, but EDS confirmed that just a few micrometres of material oxidized, Fig. 13d, presumably as a result of the high thermal conductivity of the composite.

The oxidation behaviour of $MoSi_2$ in a boride matrix follows reaction (1), whilst ZrB_2 oxidizes into zirconia and glassy boron oxide (3). Mo-based compounds have no chance of surviving at high oxygen partial pressure, therefore vaporization of the Mo oxide occurs at the composite surface (4):

$$ZrB_2 + 1.5O_{2(g)} \rightarrow ZrB_2 + B_2O_{3(g)} \quad (3)$$

$$2MoB + 4.5O_{2(g)} \rightarrow 2MoO_{3(l)} + B_2O_{3(l)} \rightarrow 2MoO_{3(g)} + B_2O_{3(g)} \quad (4)$$

Besides the oxidation of the outermost scale, whose mechanism has been thoroughly explored in previous studies [18], what is important to note with this test is that there was both no damage to the internal fibre-rich zone and minimal material recession at the surface, both of which are very desirable and support the idea that there will be minimal changes to the structural properties of the FGC.

4. Conclusions

A novel ZrB_2 functionally graded composite containing 0 to 50 vol% of carbon short fibres was successfully manufactured by a route based on simple powder mixing followed by hot pressing. The final material had a density of only 3.87 g/cm^3 and exhibited twice the flexural strength at 1500 °C, ~200 MPa, compared to room temperature, ~100 MPa, almost certainly owing to the release of residual stresses. The major achievement for the composite, however, was the magnitude of the fracture toughness exhibited. It ranged from 3.3 to 5.6 MPa m^{½} at room temperature, depending on the architecture orientation, to values from 6.0 to 8.8 MPa m^{½} at 1500 °C with overall improved failure tolerance behaviour. Plots of the specific toughness and strength further underlined that at high temperature the trade-off between strength and toughness was well overcome by the functionally graded architecture. This is possibly due to the exploitation of the favourable residual stresses arising between layers of different composition.

The functionally graded composite was also tested using an oxyacetylene torch, achieving a peak temperature of ~2500 °C. The thickness of the oxidized scale was minimal, just 45 μm, even at the centre of the disc where the flame impinged, whilst, most importantly, the fibre-free surface layer efficiently protected the composite underneath, leaving the fibres undamaged. In addition, for the first time, the real nature of the

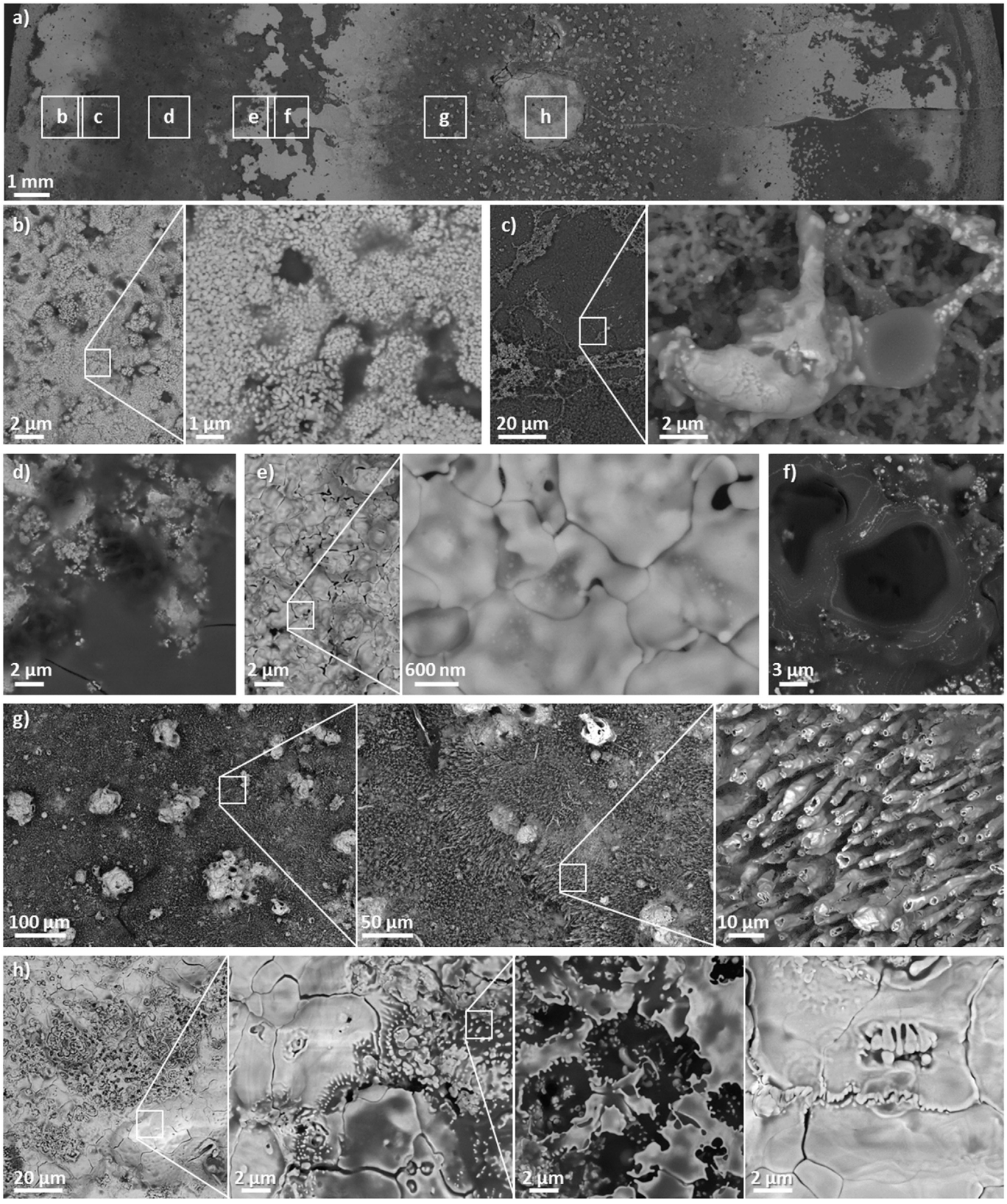

Fig. 13. SEM images of the surface of the disc after OAT testing showing (a) an overview and (b)-(h) microstructural details from regions identified in (a) with corresponding magnified views.

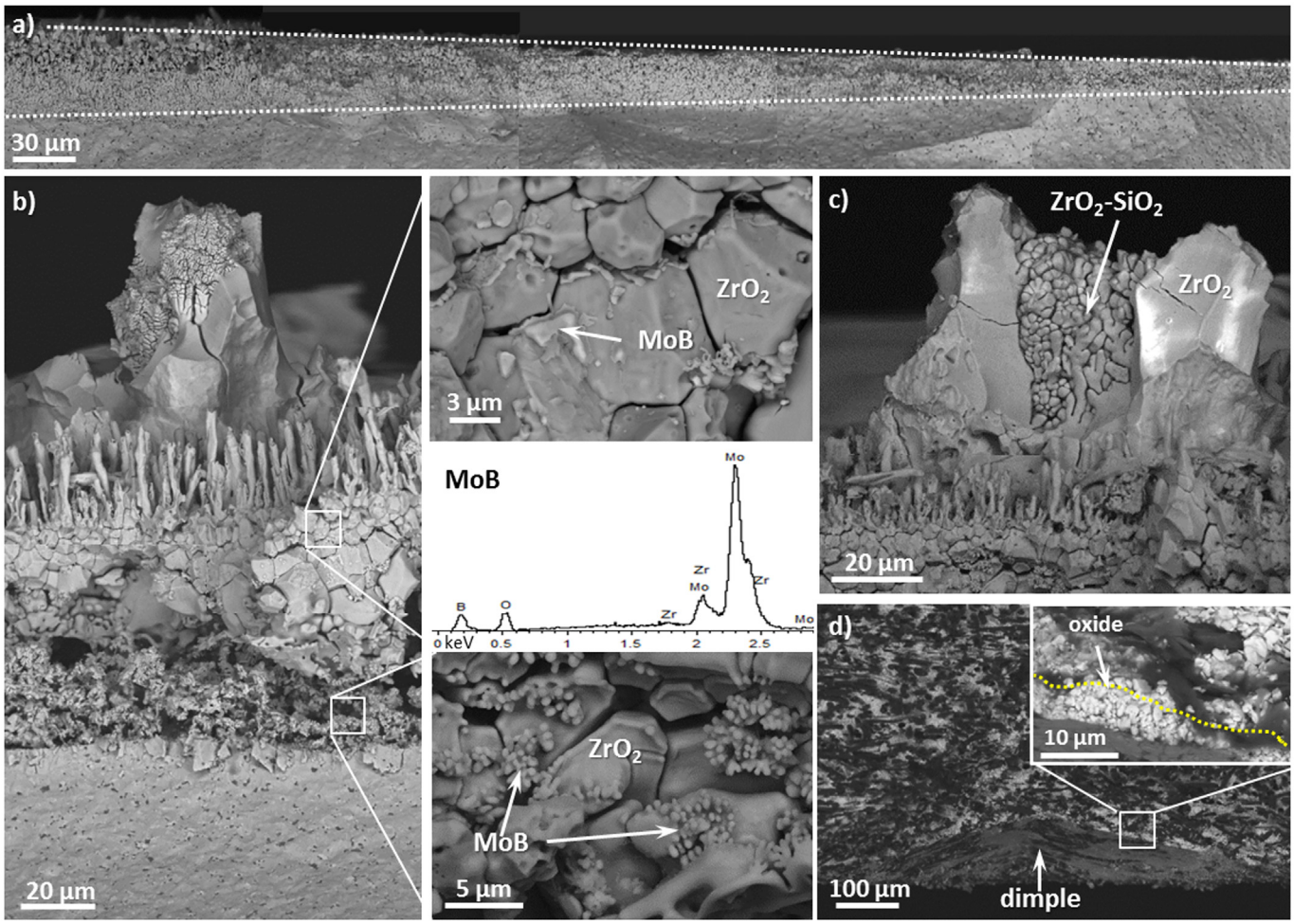

Fig. 14. SEM images of the cross section of the disc upon torch test showing (a) variable oxide thickness and microstructure details on the (b–c) front or (d) back surface. The dotted line in the inset in (d) marks the oxidized scale.

"columnar" ZrO_2 formed upon oxidation of the transition metal borides was observed, which was clearly seen to be hollow tubes.

In light of these first preliminary analyses, the FG concept applied to a UHTC matrix seems to offer a rapid and economic solution to issues encountered by materials in extreme environments, providing flaw tolerance, resistance to thermal shock and to ablation. The simplicity of the manufacturing process is also highlighted since it exploits conventional ceramic processing used for particulate ceramics and is thus potentially applicable on an industrial scale to obtain simple and even more complex shapes with functional symmetry. This composite could be therefore suitable to produce rocket nozzles, leading edges and nosecones able to resist severe temperatures encountered during hypersonic flights.

CRediT authorship contribution statement

Laura Silvestroni: Conceptualization, Methodology, Investigation, Data curation, Writing - original draft. **Cesare Melandri**: Investigation. **Vinothini Venkatachalam**: Investigation. **Jon Binner**: Writing - review & editing. **Diletta Sciti**: Funding acquisition.

Declaration of Competing Interest

The authors certify that they have NO affiliations with or involvement in any organization or entity with any financial interest or non-financial interest in the subject matter or materials discussed in this manuscript.

Acknowledgements

This research has received funding from the European Union's Horizon 2020 "Research and innovation programme" under grant agreement No. 685594 (C^3HARME).

Data availability

The raw and processed data required to reproduce these findings cannot be shared at this time due to legal or ethical reasons.

References

[1] K. Upadhyay, J.M. Yang, W.P. Hoffman, Materials for ultrahigh temperature structural application, Am. Ceram. Soc. Bull. 76 (1997) 51–56.
[2] W.G. Fahrenholtz, G.E. Hilmas, Refractory diborides of zirconium and hafnium, J. Am. Ceram. Soc. 90 (2007) 1347–1364.
[3] S.Q. Guo, Densification of ZrB_2-based composites and their mechanical and physical properties: a review, J. Europ. Ceram. Soc. 29 (2009) 995–1011.
[4] . MAX Phases and Ultra-High Temperature Ceramics for Extreme Environments, Ed. by J. Low, Y. Sakka and C. Hu. IGI Global. Hershey, PA, pp. 125–179 (2013).
[5] Ultra-High Temperature Ceramics: Materials for Extreme Environment Applications, Ed. by W. G. Fahrenholtz, E. J. Wuchina, W. E. Lee and Y. Zhou, Wiley, Inc., ISBN 0-471-9781118700785, (2014).
[6] R. Inoue, Y. Arai, Y. Kubota, Y. Kogo, K. Goto, Oxidation of ZrB_2 and its composites: a review, J. Mater. Sci. 53 (2018) 14885–14906.
[7] S.N. Karlsdottir, J.W. Halloran, Oxidation of ZrB_2-SiC: influence of SiC content on solid and liquid oxide phase formation, J. Am. Ceram. Soc. 92 (2009) 481–486.
[8] P.A. Williams, R. Sakidja, J.H. Perepezko, P. Ritt, Oxidation of ZrB_2–SiC ultra-high temperature composites over a wide range of SiC content, J. Europ. Ceram. Soc. 32 (2012) 3875–3883.

[9] P. Hu, W. Guolin, Z. Wang, Oxidation mechanism and resistance of ZrB_2–SiC composites, Corros. Sci. 51 (2009) 2724–2732.
[10] B. Nayebi, M. Shahedi Asl, M. Ghassemi Kakroudi, M. Shokouhimehr, Temperature dependence of microstructure evolution during hot pressing of ZrB_2–30 vol.% SiC composites, Int. J. Refract. Met. Hard Mater. 54 (2016) 7–13.
[11] B. Mohammadpour, Z. Ahmadi, M. Shokouhimehr, M. Shahedi Asl, Spark plasma sintering of Al-doped ZrB_2–SiC composite, Ceram. Int. 45 (2019) 4262–4267.
[12] P. Hu, Z. Wang, Flexure strength and fracture behavior of ZrB_2–SiC ultra-high temperature ceramic composites at 1800°C, J. Europ. Ceram. Soc. 30 (2010) 1021–1026.
[13] P. Hu, D. Zhang, S. Dong, Q. Qu, X. Zhang, A novel vibration-assisted slurry impregnation to fabricate Cf/ZrB_2-SiC composite with enhanced mechanical properties, J. Europ. Ceram. Soc. 39 (2019) 798–805.
[14] W.G. Fahrenholtz, Thermodynamic analysis of ZrB_2–SiC oxidation: formation of a SiC-depleted region, J. Am. Ceram. Soc. 90 (2007) 143–148.
[15] I.G. Talmy, J.A. Zaykoski, M.M. Opeka, High temperature chemistry and oxidation of ZrB_2 ceramics containing SiC, Si_3N_4, Ta_5Si_3 and $TaSi_2$, J. Am. Ceram. Soc. 91 (2008) 2250–2257.
[16] P. Hu, X.H. Zhang, J.C. Han, X.G. Luo, S.Y. Du, Effect of various additives on the oxidation behavior of ZrB_2-based ultra-high-temperature ceramics at 1800°C, J. Am. Ceram. Soc. 93 (2010) 345–349.
[17] L. Silvestroni, G. Meriggi, D. Sciti, Oxidation behavior of ZrB_2 composites doped with various transition metal silicides, Corros. Sci. 83 (2014) 281–291.
[18] L. Silvestroni, K. Stricker, D. Sciti, H.-J. Kleebe, Understanding the oxidation behavior of a ZrB_2–$MoSi_2$ composite at ultra-high temperatures, Acta Mater. 151 (2018) 216–228.
[19] R. Savino, M. De Stefano Fumo, L. Silvestroni, D. Sciti, Arc-jet testing on $HfB_2$and HfC -based ultra-high-temperature-ceramic materials, J. Europ. Ceram. Soc. 28 (2008) 1899–1907.
[20] P. Galizia, S. Failla, L. Zoli, D. Sciti, Tough salami-inspired Cf/ZrB_2 UHTCMCs produced by electrophoretic deposition, J. Eur. Ceram. Soc. 38 (2018) 403–409.
[21] L. Zoli, A. Vinci, P. Galizia, C. Melandri, D. Sciti, On the thermal shock resistance and mechanical properties of novel unidirectional UHTCMCs for extreme environments, Sci. Rep. 8 (2018) 9148.
[22] D. Sciti, S. Guicciardi, L. Silvestroni, SiC chopped fibres reinforced ZrB_2: effect of the sintering aid, Scripta Mater 64 (2011) 769–772.
[23] L. Silvestroni, D. Sciti, Oxidation of ZrB_2 ceramics containing SiC as particles, whiskers, or short fibers, J. Am. Ceram. Soc. 94 (2011) 2796–2799.
[24] L. Silvestroni, D. Dalle Fabbriche, C. Melandri, D. Sciti, Relationships between carbon fiber type and interfacial domain in ZrB_2-based ceramics, J. Europ. Ceram. Soc. 36 (2016) 17–24.
[25] M. Shahedi Asl, Y. Azizian-Kalandaragh, Z. Ahmadi, A. Sabahi Namini, A. Motallebzadeh, Spark plasma sintering of ZrB_2-based composites co-reinforced with SiC whiskers and pulverized carbon fibers, Int. J. Refract. Met. Hard Mater. 83 (2019), 104989.
[26] S. Karimirad, Z. Balak, Characteristics of spark plasma sintered ZrB_2-SiC-SCFs composites, Ceram. Int. 45 (2019) 6275–6281.
[27] M. Shahedi Asl, F. Golmohammadi, M. Ghassemi Kakroudi, M. Shokouhimehr, Synergetic effects of SiC and Csf in ZrB_2-based ceramic composites. Part I: densification behavior, Ceram. Int. 42 (2016) 4498–4506.
[28] M. Shahedi Asl, Microstructure, hardness and fracture toughness of spark plasma sintered ZrB_2–SiC–Cf composites, Ceram. Int. 43 (2017) 15047–15052.
[29] Y. Kubota, Y. Arai, M. Yano, R. Inoue, K. Goto, Y. Kogo, Oxidation and recession of plain weave carbon fiber reinforced ZrB_2-SiC-ZrC in oxygen–hydrogen torch environment, J. Europ. Ceram. Soc. 39 (2019) 2812–2823.
[30] M. Niino, T. Hirai, R. Watanabe, The functionally gradient materials, J. Jap. Soc. Comp. Mater. 13 (1987) 257–264.
[31] Z. Jin, R.C. Batra, Thermal shock resistance of functionally graded materials, Acta Mater. 52 (2004) 4961–4972.
[32] C.Y. Huang, Y.L. Chen, Design and impact resistant analysis of functionally graded Al_2O_3–ZrO_2 ceramic composite, Mater. Des. 91 (2016) 294–305.
[33] T.P.D. Rajan, B.C. Pai, Developments in processing of functionally gradient metals and metal–ceramic composites: a review, Acta Metall. Sin. 27 (2014) 825–828.
[34] O. Carvalho, M. Buciumeanu, G. Miranda, S. Madeira, F.S. Silva, Development of a method to produce FGMs by controlling the reinforcement distribution, Mater. Des. 92 (2016) 233–239.
[35] L. Silvestroni, C. Capiani, D. Dalle Fabbriche, C. Melandri, Novel light and tough ZrB_2-based functionally graded ceramics, Composites: B 99 (2016) 321–329.
[36] C. Fang, P. Hu, S. Dong, P. Xie, K. Wang, X. Zhang, Design and optimization of the coating thickness on chopped carbon fibers and sintering temperature for ZrB_2-SiC-Cf composites prepared by hot pressing, J. Europ. Ceram. Soc. 39 (2019) 2805–2811.
[37] D.G. Munz, J.L. Shannon Jr., R.T. Bubsey, Fracture toughness calculations from maximum load in four point bend tests of chevron notch specimens, Int. J. Fract. 16 (1980) R137–R141.
[38] F. Monteverde, A. Bellosi, Effect of the addition of silicon nitride on sintering behaviour and microstructure of zirconium diboride, Scripta Mater 46 (2002) 223–228.
[39] D. Sciti, L. Zoli, L. Silvestroni, A. Cecere, G.D. Di Martino, R. Savino, Design, fabrication and high velocity oxy-fuel torch tests of a Cf-ZrB_2-nozzle to evaluate its potential in rocket motors, Mater. & Design 109 (2016) 709–717.
[40] L. Náhlík, L. Šestáková, P. Hutař, R. Bermejo, Prediction of crack propagation in layered ceramics with strong interfaces, Eng. Fract. Mechanics 77 (2010) 2192–2199.
[41] R. Bermejo, Y. Torres, C. Baudin, A.J. Sánchez-Herencia, J. Pascual, M. Anglada, et al., Threshold strength evaluation on an Al_2O_3–ZrO_2 multilayered system, J. Europ. Ceram. Soc. 27 (2007) 1443–1448.
[42] J. Marschall, D. Pejakovic, W.G. Fahrenholtz, G.E. Hilmas, F. Panerai, O. Chazot, Temperature jump phenomenon during plasmatron testing of ZrB_2-SiC ultra-high temperature ceramics, J. Thermophys. Heat Transf. 26 (2012) 559–572.
[43] S. Mungiguerra, G.D. Di Martino, A. Cecere, R. Savino, L. Silvestroni, A. Vinci, L. Zoli, D. Sciti, Arc-jet wind tunnel characterization of Ultra-High-Temperature Ceramic Matrix Composites, Corros. Sci. 149 (2019) 18–28.
[44] T.A. Parthasarathy, R.A. Rapp, M. Opeka, R.J. Kerans, A model for the oxidation of ZrB_2, HfB_2 and TiB_2, Acta Mater. 55 (2007) 5999–6010.
[45] P. Hu, K. Gui, Y. Yang, S. Dong, X. Zhang, Effect of SiC content on the ablation and oxidation behavior of ZrB_2-based ultra-high temperature ceramic composites, Mater 6 (2013) 1730–1744.
[46] W.B. Han, P. Hu, X.H. Zhang, J.C. Han, S.H. Meng, High-temperature oxidation at 1900°C of ZrB_2–xSiC ultrahigh-temperature ceramic composites, J. Am. Ceram. Soc. 91 (2008) 3328–3334.
[47] R. Inoue, Y. Arai, Y. Kubota, Oxidation behaviors of ZrB_2–SiC binary composites above 2000°C, Ceram. Int. 43 (2017) 8081–8088.
[48] F. Predel, Phase diagram of Mo-O (molybdenum-oxygen) system, in: F. Predel (Ed.), Phase Equilibria, Crystallographic and Thermodynamic Data of Binary Alloys. Physical Chemistry, vol 12D, Springer, Berlin, Heidelberg, 2016.